Title

Evolution-inspired design of multicolored photoswitches from a single cyanobacteriochrome scaffold.

Journal

Proceedings of the National Academy of Sciences of the United States of America, 117(27)

ISSN

0027-8424

Authors

Fushimi, Keiji
Hasegawa, Masumi
Ito, Takeru
et al.

Publication Date

2020-07-01

DOI

10.1073/pnas.2004273117

Peer reviewed

Evolution-inspired design of multicolored photoswitches from a single cyanobacteriochrome scaffold

Keiji Fushimi[a,b,1], Masumi Hasegawa[a], Takeru Ito[a], Nathan C. Rockwell[c], Gen Enomoto[b,d], Ni-Ni -Win[d], J. Clark Lagarias[c], Masahiko Ikeuchi[b,d], and Rei Narikawa[a,b,e,1]

[a]Department of Biological Science, Faculty of Science, Shizuoka University, Suruga, Shizuoka 422-8529, Japan; [b]Core Research for Evolutional Science and Technology, Japan Science and Technology Agency, Kawaguchi, Saitama 332-0012, Japan; [c]Department of Molecular and Cellular Biology, University of California, Davis, CA 95616; [d]Graduate School of Arts and Sciences, University of Tokyo, Meguro, Tokyo 153-8902, Japan; and [e]Research Institute of Green Science and Technology, Shizuoka University, Suruga, Shizuoka 422-8529, Japan

Edited by Peter H. Quail, University of California, Berkeley, CA, and approved May 27, 2020 (received for review March 6, 2020)

Cyanobacteriochromes (CBCRs) are small, bistable linear tetrapyrrole (bilin)-binding light sensors which are typically found as modular components in multidomain cyanobacterial signaling proteins. The CBCR family has been categorized into many lineages that roughly correlate with their spectral diversity, but CBCRs possessing a conserved DXCF motif are found in multiple lineages. DXCF CBCRs typically possess two conserved Cys residues: a first Cys that remains ligated to the bilin chromophore and a second Cys found in the DXCF motif. The second Cys often forms a second thioether linkage, providing a mechanism to sense blue and violet light. DXCF CBCRs have been described with blue/green, blue/orange, blue/teal, and green/teal photocycles, and the molecular basis for some of this spectral diversity has been well established. We here characterize AM1_1499g1, an atypical DXCF CBCR that lacks the second cysteine residue and exhibits an orange/green photocycle. Based on prior studies of CBCR spectral tuning, we have successfully engineered seven AM1_1499g1 variants that exhibit robust yellow/teal, green/teal, blue/teal, orange/yellow, yellow/green, green/green, and blue/green photocycles. The remarkable spectral diversity generated by modification of a single CBCR provides a good template for multiplexing synthetic photobiology systems within the same cellular context, thereby bypassing the time-consuming empirical optimization process needed for multiple probes with different protein scaffolds.

optogenetics | phytochrome | circular dichroism

Cyanobacteriochromes (CBCRs) are single-domain light sensors that incorporate linear tetrapyrrole (bilin) chromophores such as phycoviolobilin (PVB) and phycocyanobilin (PCB) (*SI Appendix*, Fig. S1 *A* and *B*) (1, 2). Like the distantly related phytochromes, CBCRs are covalently bound to their bilins via a thioether linkage between a conserved "first Cys" (or canonical Cys) and the C3 side chain of the bilin. Both CBCRs and canonical phytochromes (3) use photoisomerization of the C15–C16 bilin double bond to trigger reversible photoconversion between their *15Z* dark state and their *15E* photoproduct state via a series of intermediates (*SI Appendix*, Fig. S1 *A* and *B*).

CBCRs exhibit a broad spectral range of photocycles from the UV to the far-red, and the molecular basis of their light-sensing properties has been extensively studied by spectroscopic and structural methods (2). A number of different CBCR subfamilies have been identified by primary sequence and phylogenetic analysis, and these subfamilies often exhibit different photocycles. Multiple CBCR lineages contain a highly conserved Asp-Xaa-Cys-Phe (DXCF) signature sequence roughly corresponding to a conserved Asp-containing motif in phytochromes (corresponding to Asp207 in the model phytochrome Cph1) (4). This motif provides DXCF CBCRs with a second conserved Cys residue or "second Cys" that plays a critical role in spectral tuning of these proteins (5–11).

Prototypical DXCF CBCRs initially incorporate PCB as chromophore precursor and then isomerize it to PVB over time to yield photoreceptors with blue-absorbing (^{15Z}Pb) dark states and green-absorbing (^{15E}Pg) photoproduct states (a blue/green photocycle; Fig. 1 *A* and *B* and *SI Appendix*, Figs. S1*C* and S2 *A* and *B*) (5, 9, 11–15). Several studies have established that the secondary structures of the protein scaffold, especially near the DXCF motif, are dynamically changed upon photoconversion (Fig. 1*C* and *SI Appendix*, Fig. S2 *A* and *B*) (16–18). The second Cys residue contributes to two important processes, i.e., PCB-to-PVB isomerization and reversible thioether linkage formation at the C10 position of the chromophore during the photoconversion cycle (5, 7, 14). Both processes shorten the π-conjugated system and strongly blue shift the absorption of the bound chromophore into the blue and violet range (*SI Appendix*, Figs. S1 *A* and *B* and S2 *A* and *B*).

Other DXCF CBCRs are unable to catalyze the PCB-to-PVB chromophore conversion or to form linkages with the second Cys residue (Fig. 1*D* and *SI Appendix*, Fig. S2*C*) (8, 9, 11, 15, 21, 22). Those unable to generate PVB exhibit blue/yellow or blue/orange photocycles instead of the prototypical blue/green DXCF CBCR photocycle (*SI Appendix*, Fig. S1*D*). This arises from the reversible photoconversion between their dual cysteine-linked ^{15E}Pb dark states and yellow-absorbing (^{15E}Py) (or orange-absorbing [^{15E}Po])

Significance

Cyanobacteriochromes (CBCRs) are small cyanobacterial photoreceptors which are highly diversified and categorized into many lineages based on their primary sequences. In this study, we identified an atypical CBCR exhibiting an orange/green reversible photocycle. Step-by-step site-directed mutagenesis was performed on this native CBCR, and seven new photoconvertible variants were created. During this process, we identified residues crucial for each color tuning event. These seven molecules covering the shorter-wavelength blue-to-orange region would contribute to the future development of multicolored optogenetic tools and are complementary to recently developed molecules sensing longer wavelengths of light.

Author contributions: K.F., M.H., N.C.R., G.E., J.C.L., M.I., and R.N. designed research; K.F., M.H., T.I., N.-N.-W., and R.N. performed research; K.F., N.C.R., G.E., and R.N. analyzed data; and K.F., N.C.R., J.C.L., and R.N. wrote the paper.

The authors declare no competing interest.

This article is a PNAS Direct Submission.

[1]To whom correspondence may be addressed. Email: fushimi.keiji@shizuoka.ac.jp or narikawa.rei@shizuoka.ac.jp.

This article contains supporting information online at https://www.pnas.org/lookup/suppl/doi:10.1073/pnas.2004273117/-/DCSupplemental.

First published June 22, 2020.

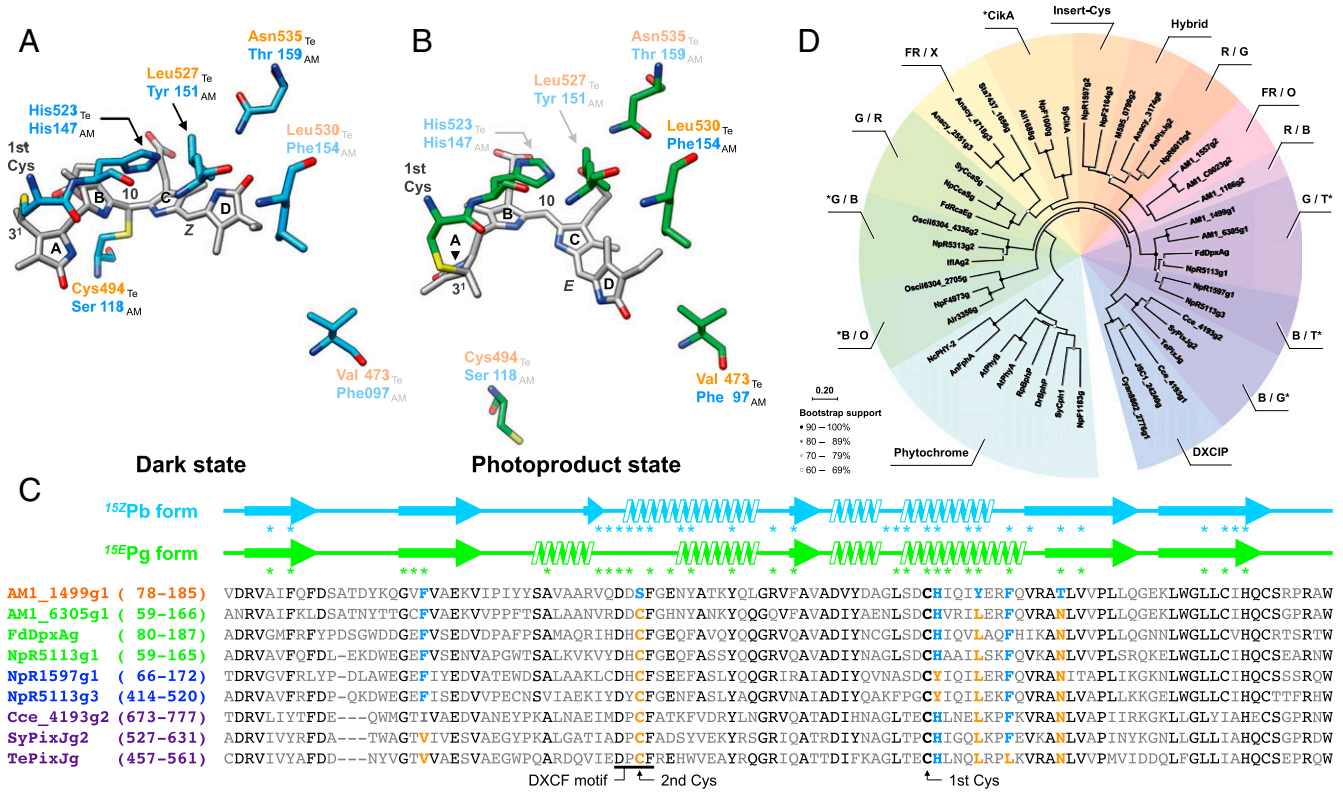

Fig. 1. Photochemical diversity of CBCRs. Crystal structures of DXCF CBCR TePixJ in (*A*) the ^{15Z}Pb form (19) (PDB ID 4GLQ; amino acid residues are shown in cyan, and chromophore is shown in gray) and (*B*) the ^{15E}Pg form (20) (PDB ID 4GLQ; amino acid residues are shown in lime green, and chromophore is shown in gray). Key mutation sites Val473, Cys494 of the second Cys, His523, Leu527, Leu530, and Asn535 in TePixJg (Te) are shown, corresponding to residues Phe97, Ser118, His147, Tyr151, Phe154, and Thr159 in AM1_1499g1 (AM). These amino acid residues are highlighted in a sequence shown below. (*C*) Sequence comparison between AM1_1499g1 (orange), green/teal (yellow green), blue/teal (blue), and blue/green (violet) CBCRs. Predicted secondary structures of the ^{15Z}Pb (cyan) and the ^{15E}Pg (lime green) forms and amino acid residues within 6 Å of the chromophores (asterisks) are based on the structures of the ^{15Z}Pb form of TePixJg (PDB ID 4GLQ) and the ^{15E}Pg form of TePixJg (PDB ID 3VV4). Amino acid residues of AM1_1499g1 mutated in this study (shown in sky blue) were substituted with residues found in other CBCRs (shown in orange). Highly conserved residues shown in black boldface type include the nearly invariant first Cys and the second Cys found in Asp-Xaa-Cys-Phe (DXCF) motif. (*D*) Phylogenetic tree of selected CBCRs and phytochromes, based on the alignment shown in *SI Appendix* and Dataset S1. Each lineage cluster is classified according to photocycle. CBCR subfamilies possessing the DXCF motif are indicated with asterisks.

photoproduct states that are red-shifted from those of photoproduct states of DXCF CBCRs with PVB chromophores (*SI Appendix*, Fig. S2 *C*, *i*). DXCF CBCRs that lack the second linkage retain the fully conjugated π systems in both dark and photoproduct states, which can absorb in the teal-to-yellow region with PVB (*SI Appendix*, Fig. S2 *C*, *ii*).

In addition to PCB-to-PVB isomerization and second linkage formation, spectral blue shifting can also occur via a trapped-twist mechanism, e.g., photoproduct states of red/green CBCRs in which the chromophore's ring D adopts a twisted geometry relative to the plane of the B and C rings (*SI Appendix*, Fig. S2 *C*, *iii*) (15, 23). DXCF CBCRs with PVB can form such a photoproduct state; formation of the second linkage in such cases results in a blue/teal photocycle, whereas absence of this linkage yields a green/teal photocycle (8, 11, 15, 21). Thus, much of the spectral diversity of DXCF CBCR photocycles can be explained by three mechanisms: 1) PCB-to-PVB isomerization, 2) reversible Cys-adduct formation, and 3) trapping of a twisted D ring in the photoproduct state (*SI Appendix*, Fig. S2*C*).

Previously, we characterized a number of CBCRs from the symbiotic cyanobacterium *Acaryochloris marina* MBIC11017 (8, 24–27). In the present study, we focus on a newly identified member of the DXCF CBCR subfamily from *A. marina*, AM1_1499g1, that lacks the second Cys residue. A close relative of AM1_6305g1, AM1_1499g1 is a member of a DXCF CBCR lineage that contains the previously studied CBCRs, FdDpxAg, NpR5113g1, NpR1597g1, and NpR5113g3 (Fig. 1*D*) (8, 11, 21). Members of this class of CBCRs exhibit teal-absorbing photoproducts with blue/teal (NpR1597g1 and NpR5113g3) and green/teal (AM1_6305g1, FdDpxAg, and NpR5113g1) photocycles. The teal-absorbing (^{15E}Pt) photoproduct states of this DXCF CBCR lineage all possess trapped-twisted PVB chromophores, whereas their distinct dark-state spectra reflect the ability (or inability) of the second Cys to form the second linkage at C10. Due to the absence of a second Cys, we reasoned that AM1_1499g1 would possess a PCB chromophore and would exhibit a photocycle distinct from that of prototypical DXCF CBCRs. The present studies establish that AM1_1499g1 has an orange/green photocycle and a singly linked PCB chromophore. We use site-directed mutagenesis of AM1_1499g1, informed by amino acid sequences of other members of this lineage, to experimentally reconstruct a pathway of molecular evolution that recapitulates most of the broad spectral palette of DXCF-containing CBCRs.

Results and Discussion

Wild-Type AM1_1499g1 Senses Orange Light with a PCB Chromophore and Exhibits Thermochromic Behavior. His-tagged AM1_1499g1 was expressed in the PCB-producing *Escherichia coli* and purified using the Ni-affinity column chromatography (*SI Appendix*, Fig. S3 *A* and *B*). Serendipitously, we observed a violet to blue color change of the purified white light-exposed solution when the solution temperature was increased (*SI Appendix*, Fig. S3*A*).

This change reflected the shift of the absorption maximum of the photoproduct from green at 5 °C to orange at 30 °C (*SI Appendix*, Fig. S4*A*). AM1_1499g1 showed reversible photoconversion between an orange-absorbing ^{15Z}Po dark state (λ_{max} = 613 nm) and a green-absorbing ^{15E}Pg photoproduct (λ_{max} = 544 nm) at 5 °C. At 30 °C, the orange-absorbing (λ_{max} = 618 nm) ^{15Z}Po dark state converted to a yellow-absorbing (λ_{max} = 589 nm) ^{15E}Py photoproduct (Figs. 2*A* and 3*A* and Table 1 and *SI Appendix*, Fig. S4*A* and Table S1). No blue- or violet-absorbing species were observed, consistent with the absence of the DXCF Cys in this protein.

To test whether PVB-to-PCB isomerization is responsible for this thermochromic behavior, we compared the normalized photochemical difference spectra (dark state – photoproduct state) of AM1_1499g1 obtained at 5 °C and 30 °C before and after denaturation (*SI Appendix*, Fig. S4*A* and Table S1). These comparisons revealed that the two difference spectra were identical after denaturation, indicating that the bound chromophore was PCB for the both preparations. Hence, PVB-to-PCB isomerization was not responsible for the temperature-dependent photoproduct spectral shift, again consistent with the absence of the second Cys residue.

It is possible that the temperature-dependent spectral shift of the AM1_1499g1 photoproduct is due to temperature-dependent pK_as of the chromophore and/or of nearby residues in the protein. However, work on the red/green CBCR NpR6012g4 has demonstrated that *15E*–PCB can be protonated in the trapped-twist green-absorbing state and can adopt a more relaxed orange-absorbing state (28, 29), so we favor the hypothesis that the chromophores of the green- and yellow-absorbing photoproduct species correspond to similarly constrained and relaxed D-ring chromophores, respectively. Formation of the more relaxed species at higher temperature could indicate that the green-absorbing species is a trapped intermediate, but our data suggest that the two photoproduct species are present at both temperatures in varying ratios. Similar heterogeneity as a function of temperature has been shown to proceed with a change in heat capacity in Cph1 (30), so it is possible that a significant change in the protein structure is responsible for the interconversion between these two photoproduct states as well.

Table 1. Spectral properties of AM1_1499g1 and its variant proteins

	Bilin pigment	Dark state (*Z*-isomer), λ_{max} (nm)	Photoproduct state (*E*-isomer), λ_{max} (nm)	Dark – photoproduct	
				Positive (nm)	Negative (nm)
WT	PCB	613	544	623	536
$S_{118}C$	PVB	577	491	577	491
$S_{118}C/Y_{151}L/T_{159}N$	PVB	559	492	561	492
$S_{118}C/H_{147}Y$	PVB	414	492	414	492
$F_{97}V$	PCB	620	585	637	521
$F_{97}V/S_{118}C$	PVB	577	514	578	505
$F_{97}V/S_{118}C/Y_{151}L/T_{159}N$	PVB	560	524	566	507
$F_{97}V/S_{118}C/H_{147}Y$	PVB	414	511	418	512

Absorption spectra of the WT protein were measured at low (5 °C) temperature whereas those of its variant proteins were measured at room temperature. Difference spectra (*15Z* dark state – *15E* photoproduct state) of their proteins were obtained from their absorption spectra.

The $S_{118}C$ Variant of AM1_1499g1 Restores PCB-To-PVB Isomerization, but Not Second Cys Linkage Formation. AM1_1499g1 is most closely related to the green/teal DXCF CBCR, AM1_6305g1, which retains the second Cys residue (Fig. 1*D*). We previously showed that AM1_6305g1 retains PCB-to-PVB isomerization activity despite its inability to form a C10 thiol adduct (8). We hypothesized that the introduction of the second Cys into AM1_1499g1, i.e., via construction of the $S_{118}C$ variant (*SI Appendix*, Fig. S3*B*), would confer the ability to isomerize PCB into PVB. Indeed, similar to AM1_6305g1, the $S_{118}C$ variant of AM1_1499g1 possessed a PVB chromophore and exhibited a yellow/teal photocycle (Figs. 2*B* and 3*A* and Table 1 and *SI Appendix*, Fig. S4*B* and Table S1). By comparison with the spectra of wild-type AM1_1499g1, both forms of $S_{118}C$ possessed significantly blue-shifted absorption maxima, consistent with their singly linked PVB chromophore (*SI Appendix*, Fig. S4 *A* and *B*). Taken together, these results indicate that introduction of the second Cys residue is sufficient to restore the PCB-to-PVB isomerization activity to the $S_{118}C$ variant of AM1_1499g1 but is insufficient for forming the second Cys linkage.

Exploiting Known DXCF CBCR Diversity to Engineer Color Tuning of the *15Z*-Dark State. The absorption maximum of the ^{15Z}Py dark state of $S_{118}C$ AM1_1499g1 unexpectedly was 20 nm red-shifted from that of the ^{15Z}Py dark state of its closest DXCF CBCR relative, AM1_6305g1 (8). By examining the TePixJg structure (16, 17), we identified Tyr151 and Thr159 in AM1_1499g1, which replace Leu and Asn residues in AM1_6305g1, TePixJg, and many other DXCF CBCRs (Fig. 1 *A* and *C*). To test the role of both residues on dark-state color tuning, we constructed these variants in the $S_{118}C$ background to obtain the $S_{118}C/Y_{151}L$ and $S_{118}C/T_{159}N$ double mutant proteins (*SI Appendix*, Fig. S5 *A–C*). Peaking in the yellow-green region (~570 nm), the dark-state absorption maxima of both variants were blue-shifted by ~10 nm relative to the $S_{118}C$ parent.

We next constructed the $S_{118}C/Y_{151}L/T_{159}N$ triple mutant variant (*SI Appendix*, Fig. S3*B*). The dark-state spectrum of this variant was even further blue-shifted than those of the double mutants, thereby establishing that the two substitutions additively affected the color-tuning of the dark state (*SI Appendix*, Fig. S5*C*). The resulting triple mutant variant exhibited a green/teal photocycle that was nearly identical to that of AM1_6305g1 (Figs. 2*C* and 3*A* and Table 1 and *SI Appendix*, Fig. S4*C* and Table S1). Reverse engineering to introduce Tyr and Thr residues into AM1_6305g1 was also performed (*SI Appendix*, Fig. S3*C*). The dark-state spectrum of the resulting AM1_6305g1_$L_{132}Y/N_{140}T$ variant was almost identical to that of AM1_1499g1 (*SI Appendix*, Fig. S6 *A* and *B* and Table S1). Taken together, these studies show that both of these residues perform crucial roles for color-tuning of the dark state.

Based on the TePixJg structure, the side chains of residues corresponding to Tyr151 and Thr159 in the AM1_1499g1_$S_{118}C$ variant are located in a good position to influence the D-ring geometry in the dark state (Fig. 1*A* and *SI Appendix*, Fig. S7*A*). Since the dark state of the $S_{118}C$ variant lacks the second linkage, unlike that of TePixJg, it is difficult to predict the structure and conformation of the $S_{118}C$ dark-state chromophore. We hypothesize that the replacements of Tyr151 and Thr159 with Leu and Asn are responsible for constraining the D ring in a twisted conformation (*SI Appendix*, Fig. S7 *B–D*). In support of this interpretation, the D-ring carbonyl of the dark-state chromophore of TePixJg appears to be constrained to an out-of-plane conformation by hydrogen bonding with the side chain of Asn535. Replacement of this Asn with Thr159, as found in AM1_1499g1, would require extensive chromophore repositioning to support

such a hydrogen bond. Replacement of Leu with Tyr151 in AM1_1499g1 also might influence the positioning of the chromophore via its ability to hydrogen bond with other residues such as His177, a strongly conserved residue known to constrain the D ring in *15Z* dark states of CBCRs and phytochromes (4, 17, 31). Indeed, the corresponding histidine residue in TePixJg, His553, participates in chromophore positioning by also forming an H bond to the D-ring carbonyl (16, 17).

A Conserved Tyr Residue Performs a Critical Role in Second Linkage Formation. We next focused on identifying residues that affect reversible Cys-adduct formation. According to our phylogenetic analyses, AM1_1499g1 and AM1_6305g1 are members of a CBCR lineage composed of the green/teal CBCRs, FdDpxAg and NpR5113g1, and the blue/teal CBCRs, NpR1597g1 and NpR5113g3 (Fig. 1*D*). From a sequence alignment and structural information, we identified residues conserved in the blue/teal CBCR lineage—a lineage that retains the ability to form reversible second Cys linkages. One of these was a Tyr residue next to the first Cys residue that is conserved only among the blue/teal CBCR lineage (Fig. 1 *A* and *C*). To determine the role of this Tyr residue in second Cys linkage formation, we replaced the His residue at this position in AM1_1499g1 with Tyr in the $S_{118}C$ variant background to construct the $S_{118}C/H_{147}Y$ variant (*SI Appendix*, Fig. S3*B*). We observed that this $S_{118}C/H_{147}Y$ variant bound PVB and exhibited reversible photoconversion between a blue-absorbing (λ_{max} = 414 nm) ^{15Z}Pb dark state and a teal-absorbing (λ_{max} = 492 nm) ^{15E}Pt photoproduct (Figs. 2*D* and 3*A* and Table 1 and *SI Appendix*, Fig. S4*D* and Table S1). Owing to the extremely blue-shifted dark state, these studies confirm the role of Tyr147 for second linkage formation in the dark state. The teal-absorbing photoproduct is consistent with the lability of the second linkage in this variant upon photoconversion.

To further examine the importance of this Tyr residue for Cys-adduct formation, we replaced the conserved His residue with Tyr at this position in the green/teal CBCR AM1_6305g1 and conversely replaced the conserved Tyr residue with His at this position in the blue/teal CBCR NpR5113g3 (*SI Appendix*, Figs. S3 *C* and *D* and S6 *A* and *C–E* and Table S1). The $H_{128}Y$ variant of AM_6305g1 absorbed blue light, whereas the $Y_{482}H$ variant of NpR5113g3 absorbed yellow light. In each case, the teal-absorbing photoproduct state spectra were almost identical to those of the wild-type parent. Fully consistent with the results for AM1_1499g1, these results indicate that this His/Tyr position is a crucial determinant for Cys-adduct formation. In TePixJg, this His residue is located directly above rings B and C (Fig. 1 *A* and *C* and *SI Appendix*, Fig. S7*A*). We hypothesize that the larger side chain of the Tyr residue helps to reposition the chromophore closer to the second Cys residue, facilitating Cys-adduct formation in the dark state (*SI Appendix*, Fig. S7 *B* and *E*). However, DXCF CBCRs from the other lineages that retain this His residue have been shown to retain the ability to form reversible Cys-adducts (8, 9, 11–13). This indicates that the role of this Tyr residue for Cys-adduct formation is context dependent and may be restricted to this specific lineage.

A Conserved Phe Residue Is Critical for *15E* Photoproduct Tuning. Based on the blue-shifted absorbance maxima of their *15E* photoproduct states, wild-type AM1_1499g1 and $S_{118}C$, $S_{118}C/Y_{151}L/T_{159}N$, and $S_{118}C/H_{147}Y$ variants likely possess chromophores with twisted, out-of-plane D-ring conformations. A previous study concluded that two conserved Phe residues in an α helix and a β sheet stabilize this twisted geometry to generate teal-absorbing photoproducts (Fig. 1 *B* and *C* and *SI Appendix*, Fig. S2 *C*, *iii*) (23). Since AM1_1499g1 also possesses both Phe residues, we substituted these two residues with Val or Leu to test their role in photoproduct spectral tuning. To do so, we used the blue/teal $S_{118}C/H_{147}Y$ background to yield the $F_{97}V/S_{118}C/H_{147}Y$ and $S_{118}C/H_{147}Y/F_{154}L$ triple mutants (*SI Appendix*, Fig. S5 *D* and *E*). Spectral measurements showed that the $F_{97}V$ replacement, but not $F_{154}L$ replacement, effectively converted the teal-absorbing photoproduct of the parent to a green-absorbing one in $F_{97}V/S_{118}C/H_{147}Y$. Based on these results, we conclude that the β-sheet Phe97 is a critical determinant for out-of-plane twisting of the D ring.

To further test this hypothesis, we expressed the four variants $F_{97}V$, $F_{97}V/S_{118}C$, $F_{97}V/S_{118}C/Y_{151}L/T_{159}N$, and $F_{97}V/S_{118}C/H_{147}Y$ (*SI Appendix*, Fig. S3*B*), each of which replaces the β-sheet Phe97 with a Val residue. The absorption spectra of these variants indicated that the $F_{97}V$ substitution had no influence on the ability of the parent construct to isomerize PCB to PVB (Fig. 2 *E–H* and Table 1 and *SI Appendix*, Fig. S4 *E–H* and Table S1). These analyses showed the $F_{97}V$ variant possessed a PCB chromophore, while PVB chromophores were present in all variants containing the $S_{118}C$ substitution. Moreover, the introduction of the $F_{97}V$ mutation afforded red-shifted photoproduct states relative to those of the parent constructs, while the dark-state spectra of each variant were nearly indistinguishable from those of their parents (Figs. 2 *E–H* and 3*B* and Table 1 and *SI Appendix*, Fig. S4 *E–H* and Table S1).

Thermochromism Is Lost in the AM1_1499g1 Variants. We next examined whether the temperature dependency of the photoproduct spectrum of wild-type AM1_1499g1 was present in the variant constructs described above (*SI Appendix*, Fig. S4*A* and Table S1). Surprisingly, none of these variants exhibited thermochromic behavior in either photostate (*SI Appendix*, Fig. S4 *B–H* and Table S1). As we described above, the thermochromic behavior of wild-type AM1_1499g1 appears to be due to a temperature-dependent equilibrium between a green-absorbing ^{15E}Pg photoproduct with a twisted D ring and a yellow-absorbing ^{15E}Py photoproduct with a less constrained chromophore. In this context, it is reasonable that the variant molecules possessing $F_{97}V$ replacement did not show temperature effects, because the $F_{97}V$ replacement abolished the twisted geometry of the D ring. All other variants possessed covalently bound PVB. The twisted A-ring geometry observed in the *15E* photoproducts of red/green CBCRs (32, 33) cannot form with PVB because of the saturated C5 methine bridge, which may disrupt this equilibrium.

To obtain further information on the D-ring conformation, we measured circular dichroism (CD) spectra of these molecules in both states (*SI Appendix*, Fig. S8 *A–H* and Table S2). All proteins showed negative CD in the visible region for both states, including wild-type AM1_1499g1 at both low (5 °C) and high (30 °C) temperatures (*SI Appendix*, Fig. S8*I* and Table S2). These results suggested that the D ring is placed toward the α face relative to the C-ring plane irrespective of thermochromism (*SI Appendix*, Fig. S8*J*) (34). The thermochromism of AM1_1499g1 thus does not arise from heterogeneous facial dispositions of the bilin D rings and may arise from some other form of heterogeneity. Such heterogeneity is well established in other phytochrome and CBCR systems (33, 35, 36).

CBCRs Provide a Useful Toolbox of Spectrally Diverse Photoswitches for Optogenetic Applications Based on a Single Protein Scaffold. Owing to their broad spectral diversity from the near UV to the near IR and their small size, CBCRs have a bright future for optogenetic tool development (2, 37). Through engineering of AM1_1499g1, we have successfully developed a broad spectral arsenal of photoswitches, all based on a single CBCR scaffold. The robust yellow/teal photocycle of the $S_{118}C$ variant offers a large spectral separation in photoproduct states (up to 90 nm) that is advantageous for strict optogenetic control. In addition, this variant fills in a spectral gap in the current palette of photoswitches that sense blue, green, and red light, e.g., flavin-based

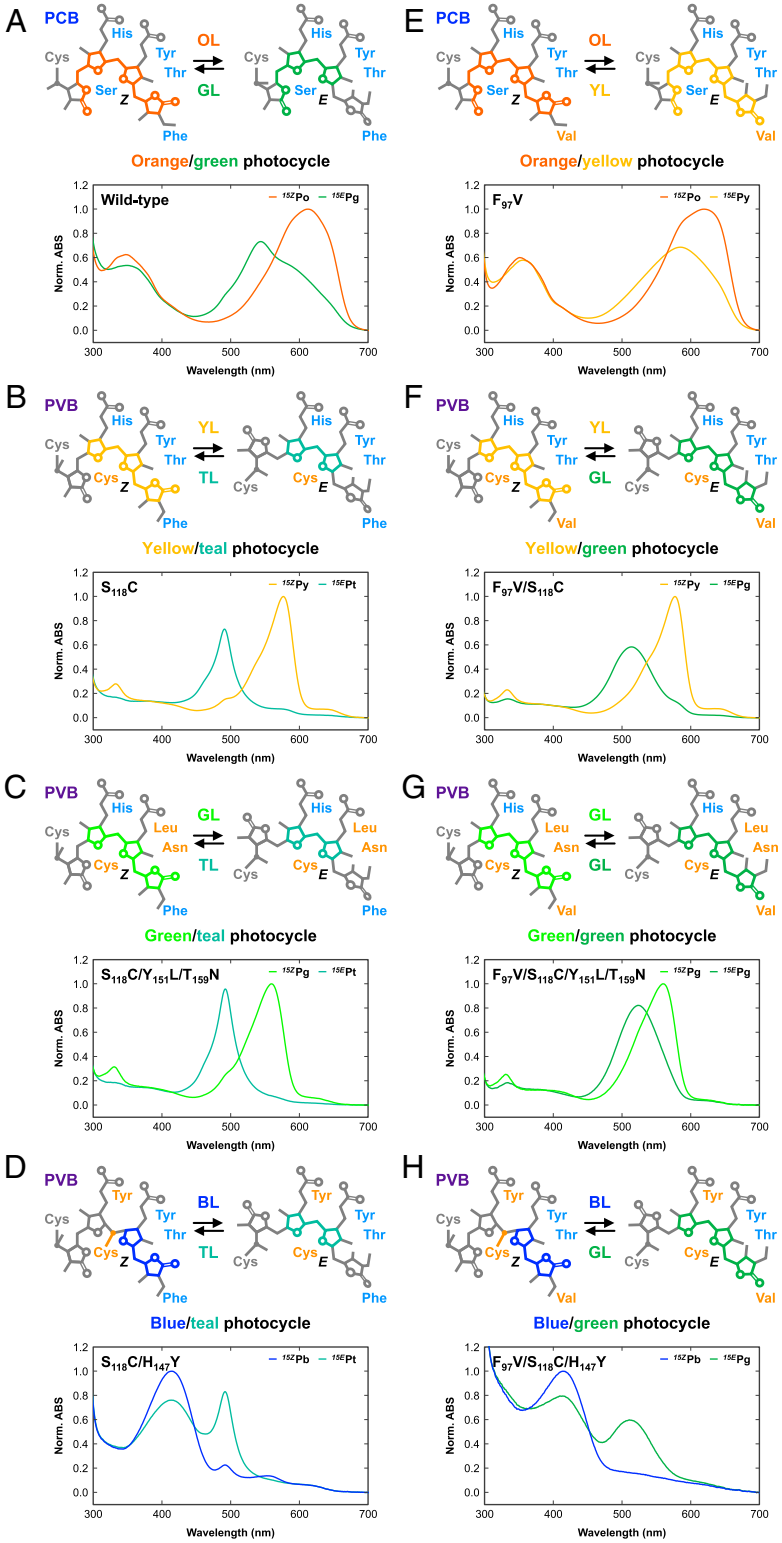

Fig. 2. Photocycles of AM1_1499g1 variants. (*A–H*) Normalized absorption spectra of AM1_1499g1 and variants are depicted with structures for each chromophore. The π-conjugated systems for each bilin are color-coded by dark-state and photoproduct-state peak absorption wavelength. (*A*) Wild-type AM1_1499g1 incorporates PCB and exhibits an orange/green photocycle at low (5 °C) temperature. (*B*) The $S_{118}C$ variant incorporates PVB and exhibits a yellow/teal photocycle. (*C*) The $S_{118}C/Y_{151}L/T_{159}N$ variant incorporates PVB and exhibits a green/teal photocycle. (*D*) The $S_{118}C/H_{147}Y$ variant incorporates PVB and exhibits a blue/teal photocycle. (*E*) The $F_{97}V$ variant incorporates PCB and exhibits an orange/yellow photocycle. (*F*) The $F_{97}V/S_{118}C$ variant incorporates PVB and exhibits a yellow/green photocycle. (*G*) The $F_{97}V/S_{118}C/Y_{151}L/T_{159}N$ variant incorporates PVB and exhibits a green/green photocycle. (*H*) The $F_{97}V/S_{118}C/H_{147}Y$ variant incorporates PVB and exhibits a blue/green photocycle. Absorption maxima are reported in Table 1. Some samples, especially the $F_{97}V/S_{118}C/H_{147}Y$ variant, showed higher absorption in the shorter-wavelength region due to scattering, indicating that these samples are unstable in solution.

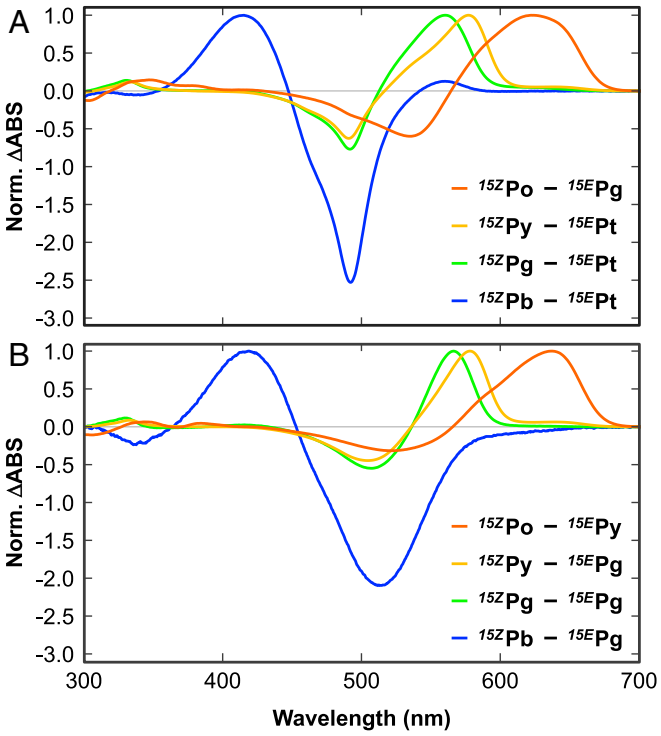

Fig. 3. Comparative photochemical difference spectra of wild-type AM1-1499g1 and its variants. Normalized difference spectra (*15Z* dark state – *15E* photoproduct state) are shown for variants with (*A*) twisted or (*B*) relaxed D-ring photoproducts. (*A*) Wild-type AM1_1499g1 (^{15Z}Po – ^{15E}Pg; orange), $S_{118}C$ (^{15Z}Py – ^{15E}Pt; yellow), $S_{118}C/Y_{151}L/T_{159}N$ (^{15Z}Pg – ^{15E}Pt; yellow-green), and $S_{118}C/H_{147}Y$ (^{15Z}Pb – ^{15E}Pt; blue). (*B*) $F_{97}V$ (^{15Z}Po – ^{15E}Py; orange), $F_{97}V/S_{118}C$ (^{15Z}Py – ^{15E}Pg; yellow), $F_{97}V/S_{118}C/Y_{151}L/T_{159}N$ (^{15Z}Pg – ^{15E}Pg; yellow-green), and $F_{97}V/S_{118}C/H_{147}Y$ (^{15Z}Pb – ^{15E}Pg; blue). Absorption maxima are reported in Table 1.

photoreceptors (38–40), cobalamin-based photoreceptors (41, 42), CBCRs (43, 44), and phytochromes (45–47).

As proof of concept, we chose to develop an optogenetic tool that leverages light to reversibly modulate the level of cyclic adenosine monophosphate (cAMP). To do so, we constructed a fusion protein between AM1_1499g1_$S_{118}C$ and the catalytic region of CyaB1, an adenylate cyclase (AC) from cyanobacterium *Anabaena* sp. PCC 7120 (*SI Appendix*, Fig. S9*A*) (48). The $S_{118}C$-AC chimera exhibited a robust yellow/teal photocycle indistinguishable from that of the $S_{118}C$ variant on its own (*SI Appendix*, Fig. S9 *B* and *C*). We measured the time course of AC activity of both forms by quantitating cAMP levels produced via HPLC analysis (*SI Appendix*, Fig. S9*D*). The ^{15Z}Py form showed about five times higher AC activity than the ^{15E}Pt form (Fig. 4 and *SI Appendix*, Table S3), establishing a proof-of-concept design principle for a new family of light-regulated cAMP optogenetic probes based on the AM1_1499g1 scaffold. It should thus be possible to develop an entire family of light-responsive adenylate cyclases with different color responses using a single AM1_1499g1 chimera with well-chosen site-directed mutagenesis rather than by laborious optimization of multiple chimeras.

Conclusions and Future Perspective. We show that AM1_1499g1 is a PCB-containing CBCR that lacks a second Cys and cannot isomerize PCB to PVB. Via structure- and sequence-informed mutagenesis that introduced PCB-to-PVB isomerization activity, second-linkage formation, and cancellation of out-of-plane trapped-twist of the bilin D ring, we generated seven variants that exhibit robust yellow/teal, green/teal, blue/teal, yellow/orange, yellow/green, green/green, and blue/green photocycles. We also leveraged one of the variant molecules to generate a chimeric molecule that reversibly regulates cAMP production under yellow and teal light. In the future, we hope to introduce mutations that were successful in altering the chromophore specificity of the red/green CBCR sensor AnPixJg2 (49), enabling substitution of PCB with biliverdin IXα, a much more widespread bilin than PCB. In principle, the lessons learned from such studies could prove useful for generation of an unprecedented palette of photoswitches based on the AM1_1499g1 scaffold for novel optogenetic applications in mammalian cells.

Materials and Methods

Bacterial Strains and Growth Media. The *E. coli* strain JM109 (TaKaRa) was used for cloning plasmid DNA, and *E. coli* strain C41 (Cosmo Bio) harboring PCB synthetic systems, pKT271, was used for protein expression as previously reported (50). Bacterial cells were grown in Lysogeny Broth (LB) medium containing 20 μg mL^{-1} kanamycin with or without 20 μg mL^{-1} chloramphenicol. For protein expression, cells were grown in LB containing the appropriate antibiotic(s) at 37 °C until the optical density at 600 nm was 0.4 to 0.8. Isopropyl β-D-1-thiogalactopyranoside (IPTG) then was added to a final concentration of 0.1 mM, and cells were cultured at 18 °C overnight.

Bioinformatic Analyses. Multiple sequence alignment and neighbor-joining phylogenetic trees were constructed with MEGA7 (Molecular Evolutionary Genetics Analysis Version 7.0) software (51). The crystal structures of PVB-bound TePixJg (^{15Z}Pb form, Protein Data Bank [PDB] ID 4GLQ; ^{15E}Pg form, PDB ID 3VV4) were utilized to assess key amino acid residues for color tuning. Molecular graphics were generated by University of California, San Francisco Chimera software (52).

Plasmid Construction. Plasmids expressing His-tagged AM1_1499g1 (amino acid positions 47 to 222) and NpR5113g3 (amino acid positions 388 to 557) (11, 15, 23) were amplified by PCR from *A. marina* MBIC11017 and *Nostoc punctiforme* PCC 73102 genomic DNA, respectively, using PrimeSTAR Max DNA polymerase (TaKaRa) and the appropriate nucleotide primers (*SI Appendix*, Table S4). AM1_6305g1 (amino acid positions 33 to 203) (8) was constructed as described in previous studies. The Gibson Assembly System (New England Biolabs) was used to fuse the cloned DNA fragments into the pET28a expression vector. The PrimeSTAR Max Basal Mutagenesis kit reagents (TaKaRa) or Kodakara Island (KOD) One PCR Master Mix (Toyobo Life Science) with appropriate nucleotide primers were used to perform site-directed mutagenesis of these proteins (*SI Appendix*, Table S4). All of the expression constructs were verified by nucleotide sequencing (FASMAC).

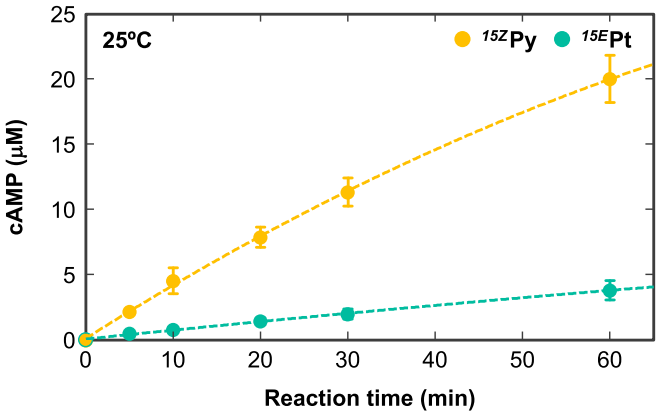

Fig. 4. Light-dependent adenylate cyclase activities of both photostates of AM1_1499g1_$S_{118}C$-AC. The enzymatic reaction catalyzing cAMP synthesis from ATP by the AM1_1499g1_$S_{118}C$–adenylate cyclase chimeric protein was examined after 0, 5, 10, 20, 30, and 60 min at 25 °C for ^{15Z}Py (yellow) and ^{15E}Pt (teal). Reaction products were quantified using HPLC (*SI Appendix*, Fig. S9*D* and Table S3). Data are reported as mean ± SD, calculated from three independent experiments.

Protein Purification. All of the proteins were expressed in *E. coli* C41 containing the bilin biosynthetic plasmid pKT271 in 1 L LB. After expression, cells were disrupted in lysis buffer [20 mM Hepes-NaOH, pH 7.5, 0.1 M NaCl and 10% (wt/vol) glycerol with or without 0.5 mM Tris(2-carboxyethyl)phosphine] using three passages through an Emulsiflex C5 high-pressure homogenizer at 12,000 psi (Avestin). Homogenates were centrifuged at 165,000 × *g* for 30 min, and supernatants were filtered through a 0.8-μm cellulose acetate membrane before loading onto a nickel-affinity His-trap column (GE Healthcare) using an ÄKTAprime plus (GE Healthcare) System. The column was washed with Lysis Buffer containing 100 mM imidazole to remove unbound proteins, and His-tagged proteins subsequently were eluted with a linear gradient of Lysis Buffer containing 100 to 400 mM imidazole (1 mL/min, total 15 min). After incubation with 1 mM EDTA for 1 h on ice, purified proteins were dialyzed against lysis buffer with or without 1 mM DTT to remove EDTA and imidazole. Protein concentrations were determined by the Bradford method.

Electrophoresis and Fluorescence Detection. Purified proteins were diluted into 60 mM Tris–HCl, pH 8.0, 2% (wt/vol) SDS, and 60 mM DTT, denatured at 95 °C for 3 min, and electrophoresed at room temperature using 12% (wt/vol) SDS polyacrylamide gels. The electrophoresed gels were soaked in distilled water for 30 min followed by visualizing fluorescence bands (details for detection of the fluorescence were described in previous studies) (48, 49) and then were stained with Coomassie Brilliant Blue R-250.

Spectroscopy. UV and visible absorption spectra of the proteins were recorded with a UV-2600 spectrophotometer (Shimadzu) at ambient temperature. AM1_1499g1 and its variant proteins were also measured at 5 and 30 °C, using a thermostated cuvette holder. Circular dichroism spectra of AM1_1499g1 and its variant proteins were recorded with a J-820 spectrophotometer (Japan Spectroscopic Corporation) at ambient temperature. Wild-type AM1_1499g1 was measured additionally at 5 and 30 °C, using a thermostated cuvette holder. An Opto-Spectrum Generator (Hamamatsu Photonics, Inc.) was used to generate monochromatic light of various wavelengths to induce photoconversion: Pb form, 400 to 430 nm; Pt form, 470 to 490 nm; Pg form, 470 to 620 nm; Py form, 490 to 640 nm; and Po form, 600 to 640 nm.

Biochemical Characterization of Cyanobacteriochromes. For denaturation assays, both dark state (*15Z*-isomer) and photoproduct state (*15E*-isomer) of the native proteins obtained at 5 or 30 °C were fivefold diluted into acidic 8 M urea, <pH 2.0, and their absorption spectra were recorded at ambient temperature before and after 3 min of illumination with white light. To assign the spectral peaks to the chromophore incorporated into each protein, those of known PCB- and PVB-binding CBCRs were recorded under the same conditions.

Light-Dependent Enzymatic Reaction of Adenylate Cyclase. The chimeric protein, AM1_1499g1_S_{118}C-AC, was constructed using the method in a previous study (48) (*SI Appendix*, Fig. S9*A*). The concentration of the purified protein was calculated using the Bradford method (Bio-Rad) using BSA as a protein standard. After photoconversion to ^{15Z}Py and ^{15E}Pt forms with saturating monochromatic light, the chimeric protein (in lysis buffer; 20 mM Hepes-NaOH, pH 7.5, 0.1 M NaCl, and 10% [wt/vol] glycerol with 1 mM DTT) was added to a reaction buffer containing ATP. The final concentrations of each component in the reaction mixture were as follows: 1 μM chimeric protein, 100 μM ATP, 50 mM Tris·HCl (pH 8.0), 50 mM NaCl, and 10 mM $MgCl_2$. Enzymatic reactions were performed at 25 °C under teal or yellow light irradiation. Aliquots were removed after 0, 5, 10, 20, 30, and 60 min, and the reaction was stopped by heating at 95 °C for 3 min. As an internal standard, nicotine adenosine dinucleotide (NAD) was added to all samples and adjusted to 1 mM as final concentration. After centrifugation, supernatants were filtered through a 0.2-μm PTFE membrane to remove insoluble aggregates. NAD, produced cAMP, and ATP in the samples were detected using a Prominence HPLC system (Shimadzu) with a reverse-phase HPLC column (Kinetex C18, 2.1 i.d. × 100 mm, 1.7 μm; Phenomenex) and eluted with a linear gradient of MeOH and phosphate buffer as described in a previous study (48). Each sample (20 μL) was injected, and absorbance at 260 nm was monitored. Quantities of accumulated cAMP by the enzymatic reaction were calculated from the ratio of the peak area of cAMP to that of NAD using standard curves. Nucleotides were assigned based on their retention times (t_R) of standard compounds.

Data Availability. The authors confirm that all data supporting the findings of this study are available within the the main text and *SI Appendix*. The sequence alignment data is provided as the Dataset S1.

ACKNOWLEDGMENTS. We thank Shelley S. Martin (University of California, Davis) for the gift of the plasmid constructs. We thank Prof. Masayuki Yazawa (Columbia University) for helpful discussion. We thank Mr. Tatsuki Masuzawa, Prof. Takanori Oyoshi, and Prof. Mitsuru Kondo (Shizuoka University) for experimental assistance. This work was supported by grants from Japan Science and Technology Agency, Core Research for Evolutional Science and Technology (JPMJCR1653 to M.I. and R.N.); from Japan Society for the Promotion of Science KAKENHI (26702036 to R.N.); and from the Chemical Sciences, Geosciences, and Biosciences Division, Office of Basic Energy Sciences, Office of Science, United States Department of Energy (DOE DE-FG02-09ER16117 to J.C.L.).

1. M. Ikeuchi, T. Ishizuka, Cyanobacteriochromes: A new superfamily of tetrapyrrole-binding photoreceptors in cyanobacteria. *Photochem. Photobiol. Sci.* **7**, 1159–1167 (2008).
2. K. Fushimi, R. Narikawa, Cyanobacteriochromes: Photoreceptors covering the entire UV-to-visible spectrum. *Curr. Opin. Struct. Biol.* **57**, 39–46 (2019).
3. N. C. Rockwell, J. C. Lagarias, Phytochrome evolution in 3D: Deletion, duplication, and diversification. *New Phytol.* **225**, 2283–2300 (2020).
4. L.-O. Essen, J. Mailliet, J. Hughes, The structure of a complete phytochrome sensory module in the Pr ground state. *Proc. Natl. Acad. Sci. U.S.A.* **105**, 14709–14714 (2008).
5. N. C. Rockwell *et al*., A second conserved GAF domain cysteine is required for the blue/green photoreversibility of cyanobacteriochrome Tlr0924 from *Thermosynechococcus elongatus*. *Biochemistry* **47**, 7304–7316 (2008).
6. N. C. Rockwell, S. S. Martin, K. Feoktistova, J. C. Lagarias, Diverse two-cysteine photocycles in phytochromes and cyanobacteriochromes. *Proc. Natl. Acad. Sci. U.S.A.* **108**, 11854–11859 (2011).
7. T. Ishizuka *et al*., The cyanobacteriochrome, TePixJ, isomerizes its own chromophore by converting phycocyanobilin to phycoviolobilin. *Biochemistry* **50**, 953–961 (2011).
8. M. Hasegawa *et al*., Molecular characterization of DXCF cyanobacteriochromes from the cyanobacterium *Acaryochloris marina* identifies a blue-light power sensor. *J. Biol. Chem.* **293**, 1713–1727 (2018).
9. Q. Ma *et al*., A rising tide of blue-absorbing biliprotein photoreceptors: Characterization of seven such bilin-binding GAF domains in *Nostoc* sp. PCC7120. *FEBS J.* **279**, 4095–4108 (2012).
10. S. M. Cho *et al*., Genomic survey and biochemical analysis of recombinant candidate cyanobacteriochromes reveals enrichment for near UV/violet sensors in the halotolerant and alkaliphilic cyanobacterium *Microcoleus* IPPAS B353. *J. Biol. Chem.* **290**, 28502–28514 (2015).
11. N. C. Rockwell, S. S. Martin, A. G. Gulevich, J. C. Lagarias, Phycoviolobilin formation and spectral tuning in the DXCF cyanobacteriochrome subfamily. *Biochemistry* **51**, 1449–1463 (2012).
12. S. Yoshihara, M. Katayama, X. Geng, M. Ikeuchi, Cyanobacterial phytochrome-like PixJ1 holoprotein shows novel reversible photoconversion between blue- and green-absorbing forms. *Plant Cell Physiol.* **45**, 1729–1737 (2004).
13. T. Ishizuka *et al*., Characterization of cyanobacteriochrome TePixJ from a thermophilic cyanobacterium *Thermosynechococcus elongatus* strain BP-1. *Plant Cell Physiol.* **47**, 1251–1261 (2006).
14. T. Ishizuka, R. Narikawa, T. Kohchi, M. Katayama, M. Ikeuchi, Cyanobacteriochrome TePixJ of *Thermosynechococcus elongatus* harbors phycoviolobilin as a chromophore. *Plant Cell Physiol.* **48**, 1385–1390 (2007).
15. N. C. Rockwell, S. S. Martin, J. C. Lagarias, Mechanistic insight into the photosensory versatility of DXCF cyanobacteriochromes. *Biochemistry* **51**, 3576–3585 (2012).
16. R. Narikawa *et al*., Structures of cyanobacteriochromes from phototaxis regulators AnPixJ and TePixJ reveal general and specific photoconversion mechanism. *Proc. Natl. Acad. Sci. U.S.A.* **110**, 918–923 (2013).
17. E. S. Burgie, J. M. Walker, G. N. Phillips Jr., R. D. Vierstra, A photo-labile thioether linkage to phycoviolobilin provides the foundation for the blue/green photocycles in DXCF-cyanobacteriochromes. *Structure* **21**, 88–97 (2013).
18. C. C. Cornilescu *et al*., Dynamic structural changes underpin photoconversion of a blue/green cyanobacteriochrome between its dark and photoactivated states. *J. Biol. Chem.* **289**, 3055–3065 (2014).
19. E. S. Burgie, J. M. Walker, G. N. Phillips Jr, R. D. Vierstra, Crystal Structure of the blue-light absorbing form of the Thermosynechococcus elongatus PixJ GAF-domain. Protein Data Bank. https://www.rcsb.org/structure/4GLQ. Deposited 14 August 2012.
20. T. Ishizuka, R. Narikawa, N. Muraki, T. Shiba, G. Kurisu, M. Ikeuchi, Crystal structure of cyanobacteriochrome TePixJ GAF domain. Protein Data Bank. https://www.rcsb.org/structure/3VV4. Deposited 14 July 2012.
21. L. B. Wiltbank, D. M. Kehoe, Two cyanobacterial photoreceptors regulate photosynthetic light harvesting by sensing teal, green, yellow, and red light. *MBio* **7**, e02130-e15 (2016).
22. N. C. Rockwell, S. S. Martin, J. C. Lagarias, Identification of DXCF cyanobacteriochrome lineages with predictable photocycles. *Photochem. Photobiol. Sci.* **14**, 929–941 (2015).
23. N. C. Rockwell, S. S. Martin, A. G. Gulevich, J. C. Lagarias, Conserved phenylalanine residues are required for blue-shifting of cyanobacteriochrome photoproducts. *Biochemistry* **53**, 3118–3130 (2014).

24. R. Narikawa, G. Enomoto, K. Ni-Ni-Win, K. Fushimi, M. Ikeuchi, A new type of dual-Cys cyanobacteriochrome GAF domain found in cyanobacterium Acaryochloris marina, which has an unusual red/blue reversible photoconversion cycle. *Biochemistry* **53**, 5051–5059 (2014).
25. R. Narikawa *et al*., A biliverdin-binding cyanobacteriochrome from the chlorophyll *d*-bearing cyanobacterium *Acaryochloris marina*. *Sci. Rep.* **5**, 7950 (2015).
26. R. Narikawa, K. Fushimi, M. Ni-Ni-Win, M. Ikeuchi, Red-shifted red/green-type cyanobacteriochrome AM1_1870g3 from the chlorophyll d-bearing cyanobacterium Acaryochloris marina. *Biochem. Biophys. Res. Commun.* **461**, 390–395 (2015).
27. K. Fushimi *et al*., Photoconversion and fluorescence properties of a red/green-type cyanobacteriochrome AM1_C0023g2 that binds not only phycocyanobilin but also biliverdin. *Front. Microbiol.* **7**, 588 (2016).
28. N. C. Rockwell, S. S. Martin, S. Lim, J. C. Lagarias, J. B. Ames, Characterization of red/green cyanobacteriochrome NpR6012g4 by solution nuclear magnetic resonance spectroscopy: A protonated bilin ring system in both photostates. *Biochemistry* **54**, 2581–2600 (2015).
29. N. C. Rockwell, S. S. Martin, S. Lim, J. C. Lagarias, J. B. Ames, Characterization of red/green cyanobacteriochrome NpR6012g4 by solution nuclear magnetic resonance spectroscopy: A hydrophobic pocket for the C15-*E,anti* chromophore in the photoproduct. *Biochemistry* **54**, 3772–3783 (2015).
30. P. W. Kim, N. C. Rockwell, S. S. Martin, J. C. Lagarias, D. S. Larsen, Dynamic inhomogeneity in the photodynamics of cyanobacterial phytochrome Cph1. *Biochemistry* **53**, 2818–2826 (2014).
31. J. R. Wagner, J. S. Brunzelle, K. T. Forest, R. D. Vierstra, A light-sensing knot revealed by the structure of the chromophore-binding domain of phytochrome. *Nature* **438**, 325–331 (2005).
32. X. Xu *et al*., Structural elements regulating the photochromicity in a cyanobacteriochrome. *Proc. Natl. Acad. Sci. U.S.A.* **117**, 2432–2440 (2020).
33. S. Lim *et al*., Correlating structural and photochemical heterogeneity in cyanobacteriochrome NpR6012g4. *Proc. Natl. Acad. Sci. U.S.A.* **115**, 4387–4392 (2018).
34. N. C. Rockwell, L. Shang, S. S. Martin, J. C. Lagarias, Distinct classes of red/far-red photochemistry within the phytochrome superfamily. *Proc. Natl. Acad. Sci. U.S.A.* **106**, 6123–6127 (2009).
35. C. Song *et al*., Two ground state isoforms and a chromophore D-ring photoflip triggering extensive intramolecular changes in a canonical phytochrome. *Proc. Natl. Acad. Sci. U.S.A.* **108**, 3842–3847 (2011).
36. F. Velazquez Escobar *et al*., Protonation-dependent structural heterogeneity in the chromophore binding site of cyanobacterial phytochrome Cph1. *J. Phys. Chem. B* **121**, 47–57 (2017).
37. T. Ziegler, A. Möglich, Photoreceptor engineering. *Front. Mol. Biosci.* **2**, 30 (2015).
38. M. Yazawa, A. M. Sadaghiani, B. Hsueh, R. E. Dolmetsch, Induction of protein-protein interactions in live cells using light. *Nat. Biotechnol.* **27**, 941–945 (2009).
39. M. J. Kennedy *et al*., Rapid blue-light-mediated induction of protein interactions in living cells. *Nat. Methods* **7**, 973–975 (2010).
40. F. Kawano, H. Suzuki, A. Furuya, M. Sato, Engineered pairs of distinct photoswitches for optogenetic control of cellular proteins. *Nat. Commun.* **6**, 6256 (2015).
41. S. Kainrath, M. Stadler, E. Reichhart, M. Distel, H. Janovjak, Green-light-induced inactivation of receptor signaling using cobalamin-binding domains. *Angew. Chem. Int. Ed. Engl.* **56**, 4608–4611 (2017).
42. C. Chatelle *et al*., A green-light-responsive system for the control of transgene expression in mammalian and plant cells. *ACS Synth. Biol.* **7**, 1349–1358 (2018).
43. J. J. Tabor, A. Levskaya, C. A. Voigt, Multichromatic control of gene expression in *Escherichia coli*. *J. Mol. Biol.* **405**, 315–324 (2011).
44. S. Senoo, S. T. Tandar, S. Kitamura, Y. Toya, H. Shimizu, Light-inducible flux control of triosephosphate isomerase on glycolysis in Escherichia coli. *Biotechnol. Bioeng.* **116**, 3292–3300 (2019).
45. S. Shimizu-Sato, E. Huq, J. M. Tepperman, P. H. Quail, A light-switchable gene promoter system. *Nat. Biotechnol.* **20**, 1041–1044 (2002).
46. A. Levskaya, O. D. Weiner, W. A. Lim, C. A. Voigt, Spatiotemporal control of cell signalling using a light-switchable protein interaction. *Nature* **461**, 997–1001 (2009).
47. E. Reichhart, A. Ingles-Prieto, A.-M. Tichy, C. McKenzie, H. Janovjak, A phytochrome sensory domain permits receptor activation by red light. *Angew. Chem. Int. Ed. Engl.* **55**, 6339–6342 (2016).
48. K. Fushimi, G. Enomoto, M. Ikeuchi, R. Narikawa, Distinctive properties of dark reversion kinetics between two red/green-type cyanobacteriochromes and their application in the photoregulation of cAMP synthesis. *Photochem. Photobiol.* **93**, 681–691 (2017).
49. K. Fushimi *et al*., Rational conversion of chromophore selectivity of cyanobacteriochromes to accept mammalian intrinsic biliverdin. *Proc. Natl. Acad. Sci. U.S.A.* **116**, 8301–8309 (2019).
50. K. Mukougawa, H. Kanamoto, T. Kobayashi, A. Yokota, T. Kohchi, Metabolic engineering to produce phytochromes with phytochromobilin, phycocyanobilin, or phycoerythrobilin chromophore in *Escherichia coli*. *FEBS Lett.* **580**, 1333–1338 (2006).
51. S. Kumar, G. Stecher, K. Tamura, MEGA7: Molecular evolutionary genetics analysis version 7.0 for bigger datasets. *Mol. Biol. Evol.* **33**, 1870–1874 (2016).
52. E. F. Pettersen *et al*., UCSF Chimera—A visualization system for exploratory research and analysis. *J. Comput. Chem.* **25**, 1605–1612 (2004).